JGR Atmospheres

RESEARCH ARTICLE
10.1029/2019JD031508

The Spatial Evolution of Upward Positive Stepped Leaders Initiated From a 356-m-Tall Tower in Southern China

Yan Gao[1], Mingli Chen[1], Zilong Qin[1], Zongxu Qiu[2], Yuexin Yang[2], Ya-ping Du[1], Shaoyang Wang[1], and Ge Zhang[1]

[1]Department of Building Service Engineering, The Hong Kong Polytechnic University, Hong Kong, [2]Shenzhen Meteorological Services Center, Shenzhen, China

Key Points:
- Two upward positive stepped leaders initiated from a tall tower were analyzed based on magnetic field and high-speed camera measurements
- The leader step length and step extension speed were found in the range of 0.5–3 m and 10^5–10^6 m/s, respectively
- The leader channel had an expanding and shrinking feature and an increasing trend with height in the range of 2–10 m

Correspondence to:
M. Chen,
mingli.chen@polyu.edu.hk

Citation:
Gao, Y., Chen, M., Qin, Z., Qiu, Z., Yang, Y., Du, Y.-p., et al. (2020). The spatial evolution of upward positive stepped leaders initiated from a 356-m-tall tower in Southern China. *Journal of Geophysical Research: Atmospheres*, *125*, e2019JD031508. https://doi.org/10.1029/2019JD031508

Received 18 AUG 2019
Accepted 2 JAN 2020
Accepted article online 6 JAN 2020

Author Contributions:
Conceptualization: Mingli Chen
Data curation: Zilong Qin, Zongxu Qiu, Yuexin Yang, Ya-ping Du, Shaoyang Wang, Ge Zhang
Formal analysis: Yan Gao, Zilong Qin
Funding acquisition: Mingli Chen
Investigation: Mingli Chen, Zilong Qin, Zongxu Qiu, Yuexin Yang, Shaoyang Wang, Ge Zhang
Methodology: Yan Gao, Mingli Chen
Project administration: Mingli Chen, Zongxu Qiu, Ya-ping Du
Resources: Mingli Chen, Zongxu Qiu, Yuexin Yang, Ya-ping Du, Shaoyang Wang, Ge Zhang
Software: Yan Gao
Supervision: Mingli Chen, Ya-ping Du
Validation: Mingli Chen
Writing - original draft: Yan Gao
Writing – review & editing: Mingli Chen

Abstract Two initial upward positive leaders (UPLs) in upward negative flashes initiated from a 356-m-tall tower were observed with a high-speed camera, an electric field sensor, and a magnetic field sensor. Although the waveforms of electric fields measured were saturated, both camera images and magnetic fields showed that the two UPLs had obvious stepwise characteristics in their upward moving stage. The magnetic fields associated with the UPLs were characterized by a series of fast-changing bipolar impulses superimposed on a slowly increasing continuous component as the leaders moved upward, which were well corresponding to the light intensity changes of their high-speed camera images. The 2-D step length and step extension speed of the two leaders were estimated in the range of 0.5–3 m and 1.1–9.4 × 10^5 m/s, respectively. The radius of the leader luminous channel as a function of time and height was also estimated. The channel radius showed first a stable increasing trend in the leader upward moving stage and then 4–5 times of shrinking and expanding processes after the leader connected the cloud. The channel expanding and shrinking speeds were in the range of 2–9 × 10^4 m/s. Particularly, the channel radius showed an obvious increasing trend with the increase of the height all the time, which was in the range of 2.8–3.5 m when around the tower tip and of 5.6–8.4 m when at 24 m high above the tower tip. Such a feature of the channel radius is in good agreement with the concept of leader corona sheath in literature.

1. Introduction

An upward negative flash is usually initiated by an upward positive leader (UPL) from a protruding ground object and transports negative charge from cloud to ground. The UPL and initial continuous current (ICC) process constitute the initial stage of an upward negative flash (Rakov & Uman, 2003).

So far, most observations of UPL were focused on its spatial extension speed, which was reported in the range of 10^4–10^6 m/s with the average being about 10^5 m/s (Gao et al., 2014; Jiang et al., 2013; Lu et al., 2013, 2015; Warner, 2010). Researchers also noticed the stepwise propagation characteristics of UPL and gave some results on the interstep interval, step length, and average speed of UPL (Biagi et al., 2011; Jiang et al., 2013; Wang et al., 2016).

Electrical characteristics, such as the maximum current, charge transferred, and duration of upward flashes with UPLs, were presented by Berger (1978). With the current derivative measurements at the top of the Peissenberg tower in Germany, Fuchs et al. (1998) reported some statistics for various parameters of the ICC pulses and return-stroke pulses in upward flashes. There were also some works on currents and electric fields associated with upward lightning flashes initiated for other instrumented towers like the Gaisberg Tower and Säntis Tower (Diendorfer et al., 2009; He et al., 2018; Romero et al., 2013; Zhou et al., 2012).

Many researchers also used various antennas to obtain the electrical and magnetic fields due to lightning strikes to tall objects in early years (Krider & Noggle, 1975; Uman et al., 1975). The characteristics of electrical and magnetic signals during the initial stage of a rocket-triggered lightning flash were well reported in works of Lu et al. (2016) and Fan et al. (2018). And the relationship between the channel luminosities and magnetic fields of lightning flashes to tall towers was presented by Chen et al. (2019).

Researchers are also interested in the channel structure of UPL. It is generally thought that a leader channel is composed of a conductive core surrounded by a corona sheath. The leader core is ionized very well and is

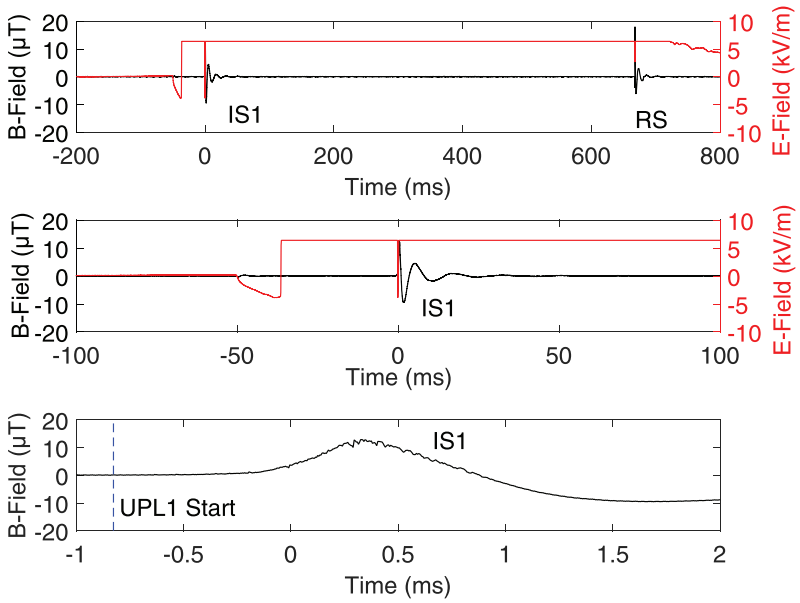

Figure 1. The overall electric and magnetic field data for an upward flash (F1603) occurred at 15:23:22, 30 July 2016, from SZMGT. The black and red curves represent the magnetic field and the electric field (saturated), respectively. IS1 is used to designate the initial stage of F1603, which included an upward positive leader (UPL1), followed by an initial continuous current (ICC1) process. RS is used to designate a subsequent leader-return-stroke process in F1603. Time 0 refers to the triggered time of the high-speed camera for F1603.

highly conductive with a small radius of several centimeters. When leader charge is deposited on the thin channel core, it will create a strong radial electric field that pushes the charge away from the core to form a corona sheath (Maslowski & Rakov, 2006).

Some laboratory experiments were done to study the distribution of the deposited charge in the corona sheath and the transition process from a leader to a return stroke (Arima et al., 1998; Cabrera & Cooray, 1992). The experiments showed that the neutralization of the space charge could take place through the action of streamer discharges moving out from the high-voltage electrode with speeds of the order of 10^5 m/s. Takagi et al. (1998) used a high-speed line-scanning camera to measure the radial variation of optical intensity of lightning channels.

A lot of numerical models were built to study the characteristics of the lightning channel corona sheath, such as sheath radius, sheath expansion velocity, and corona current (Maslowski & Rakov, 2006; Maslowski et al., 2011; Maslowski & Rakov, 2013; Xu & Chen, 2013; Chan et al., 2018).

In this paper, we present two initial UPLs in upward negative flashes initiated from a 356-m-tall tower. A high-speed camera (HC), a slow electric field antenna, and a magnetic loop antenna were used in the observation of these two flashes. Based on the simultaneous HC and magnetic field measurements, the channel extension and expansion properties of these two UPLs have been examined, as reported in detail in the following sections.

2. Experiment Setup and the Lightning Data

2.1. Experiment Setup

In 2015, a 356-m-tall Shenzhen Meteorological Gradient Tower (SZMGT) was built in Shenzhen, China. To study the initiation and attachment process of upward flashes to SZMGT, a lightning observation site was set up in 2016 on the roof of a 10-m-tall building located 440 m away from the tower base.

At the observation site, a HC was installed to capture the images of lightning events occurring around the tip of SZMGT. The HC was operated at sampling rates of 150,000 frames per second (fps) with an exposure time of 6.18 μs per frame. The focal length of the lens, the size of each pixel, and the resolution of the HC were 50

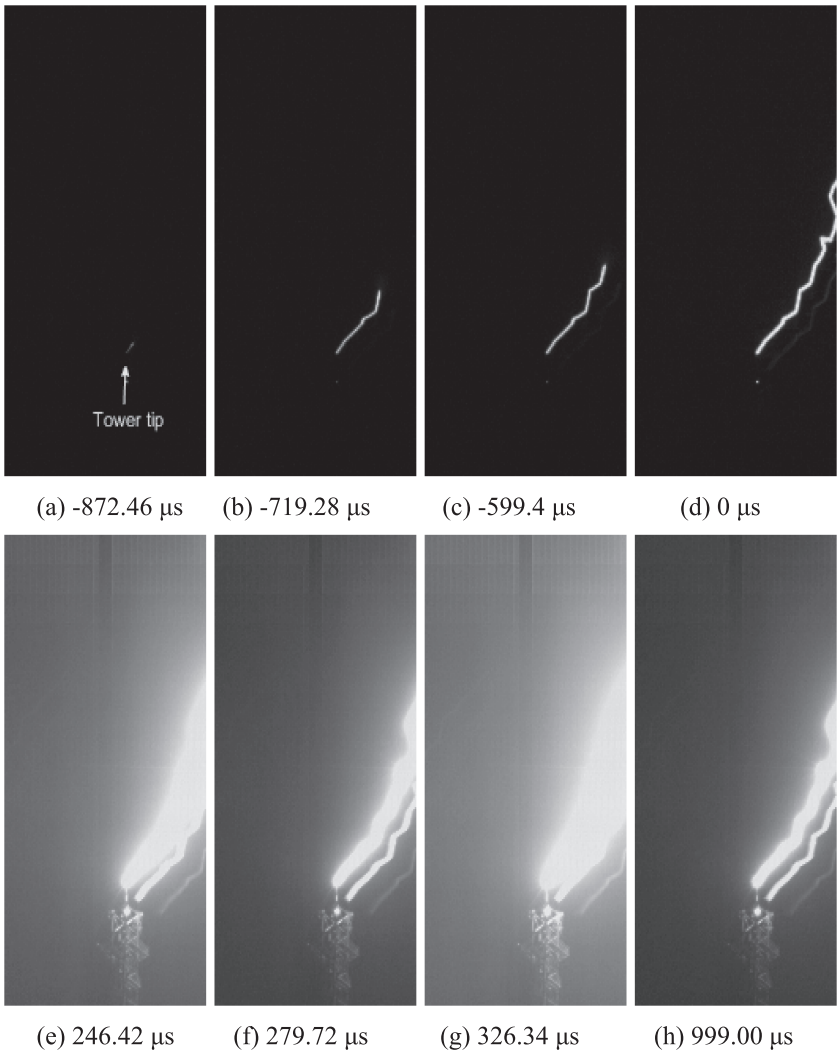

Figure 2. High-speed images for the initial upward positive leader (UPL1) and continuous current (ICC1) process for F1603, that is, IS1 in Figure 1. Panel (a) is the first frame the camera saw UPL1, (b)–(d) are three frames in the UPL1 stage, and (e)–(h) are four frames after UPL1 connected the cloud in the ICC1 stage. The weaker channel on the rightside in each panel of (d)–(h) is due to window glass reflections in the observation room. The time here is the exposure time for each frame of the camera image.

mm, 20 μm × 20 μm, and 256 × 128 pixels, respectively. The resolution of the HC at the tower tip is about 0.22 m per pixel.

A slow electric field antenna and a magnetic field antenna (MA) were also installed at the observation site to measure the electric and magnetic field changes during lightning discharges. Slow electric field antenna had a bandwidth of 0.03 Hz to 3.2 MHz with a time constant of 5.6 s. MA consisted of two crossed loops (A and B) with a bandwidth of 80 Hz to 250 kHz and a time constant of 2 ms. Loop A was installed in a way that the plane of the loop was parallel to the direction from south to north, and Loop B was parallel to the direction from east to west. The angle between the plane of Loop A and the direction to the tower was about 27°. As a result, Loop A was more sensitive to flashes to SZMGT than Loop B. Therefore, only the records of Loop A were used in the present study.

The outputs of both antennas were digitized and logged by a self-designed recording system with a digitalizing rate of five megasamples per second at 12 bits, a recording time of 1,667 ms and a 20% pretrigger time. Although some amount of aliasing is expected (since five megasamples per second $< 2 * 3.2$ MHz), the spectrum of the close E field beyond 2 MHz is expected to be small since it is dominated by the electrostatic

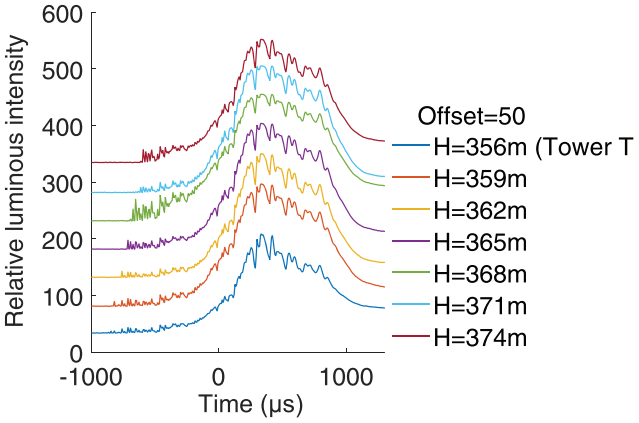

Figure 3. The relative luminous intensity versus time at seven different heights, plotted from the camera images for the initial upward positive leader (UPL1) and continuous current (ICC1) process for flash F1603, that is, IS1 in Figure 1. The tower tip is 356 m high above ground. There is an offset of 50 between the curves for easy reading.

component. One channel of the recording system was used to receive the GPS timing signal with a time uncertainty of about 100 ns. The same GPS timing signal was also input to the HC to provide a time stamp on the triggering time of each event. As such, all measurements in the experiment were synchronized with the same GPS.

2.2. Lightning Data

There are two flashes (F1603 and F1605) to be presented in this study. Both of them were upward negative flashes initiated with UPLs from the top of SZMGT.

2.2.1. Case 1 (F1603)

F1603 was an upward flash that occurred at 15:23:22, 30 July 2016, with its electric and magnetic field changes shown in Figure 1. It can be seen from the electric field changes that a nearby discharge occurred 50 ms before the start of F1603, indicating that F1603 was an other-triggered type of upward flash, rather than a self-initiated one. F1603 included two subprocesses, labeled as IS1 and RS in the figure, respectively. IS1 is used to designate the initial stage of F1603, which included an initial UPL1 started at the tip of SZMGT, followed by an ICC1 process. RS is used to designate a downward leader-upward return-stroke sequence, which occurred at 670 ms after IS1. Only the initial stage IS1 will be analyzed in detail in the following sections.

It is noted that there was a ringing distortion in magnetic field at the end of each of the IS1 and RS processes. The period of the ringing is about 12.5 ms, corresponding to 80 Hz the lower cutoff frequency of MA (a time constant of 2 ms). This is because that for a continuous current process longer than 2 ms, the MA measurement will cut off at 80 Hz, resulting in a ringing distortion after the first 2-ms stage of the continuous current process. Such a ringing will not appear if the lower cutoff frequency of the MA is low enough (say 1 Hz) to cover the whole bands of the continuous current process, or high enough (say 500 Hz) to be out of the bands

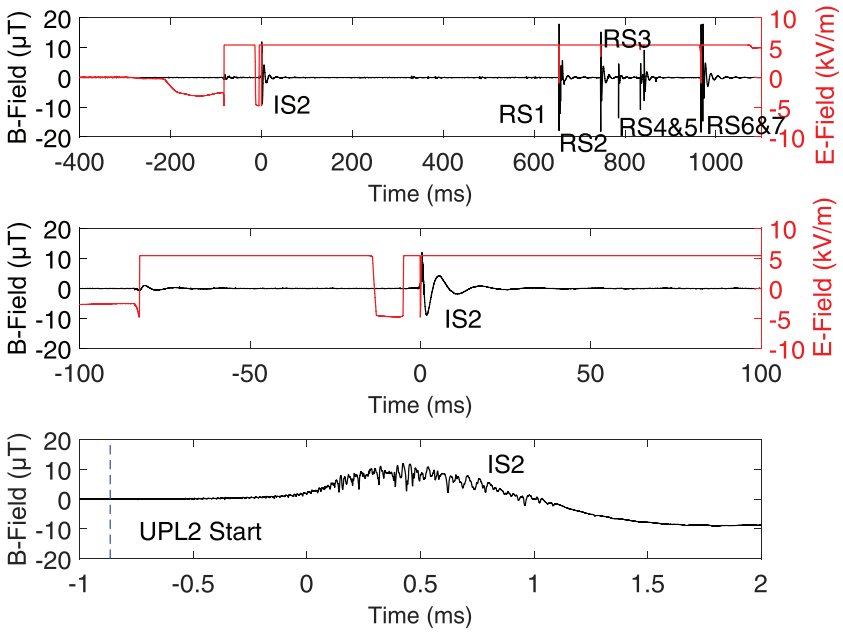

Figure 4. The overall electric and magnetic field data for the upward flash (F1605) occurred at 15:35:39, 30 July 2016, from SZMGT. The black and red curves represent the magnetic field and the electric field (saturated), respectively. IS2 is used to designate the initial stage of F1605, which included an upward positive leader (UPL2) followed by an initial continuous current (ICC2) process, while RS1–RS7 refer to seven subsequent leader-return-stroke processes following IS2. Time 0 refers to the triggered time of the high-speed camera for F1605.

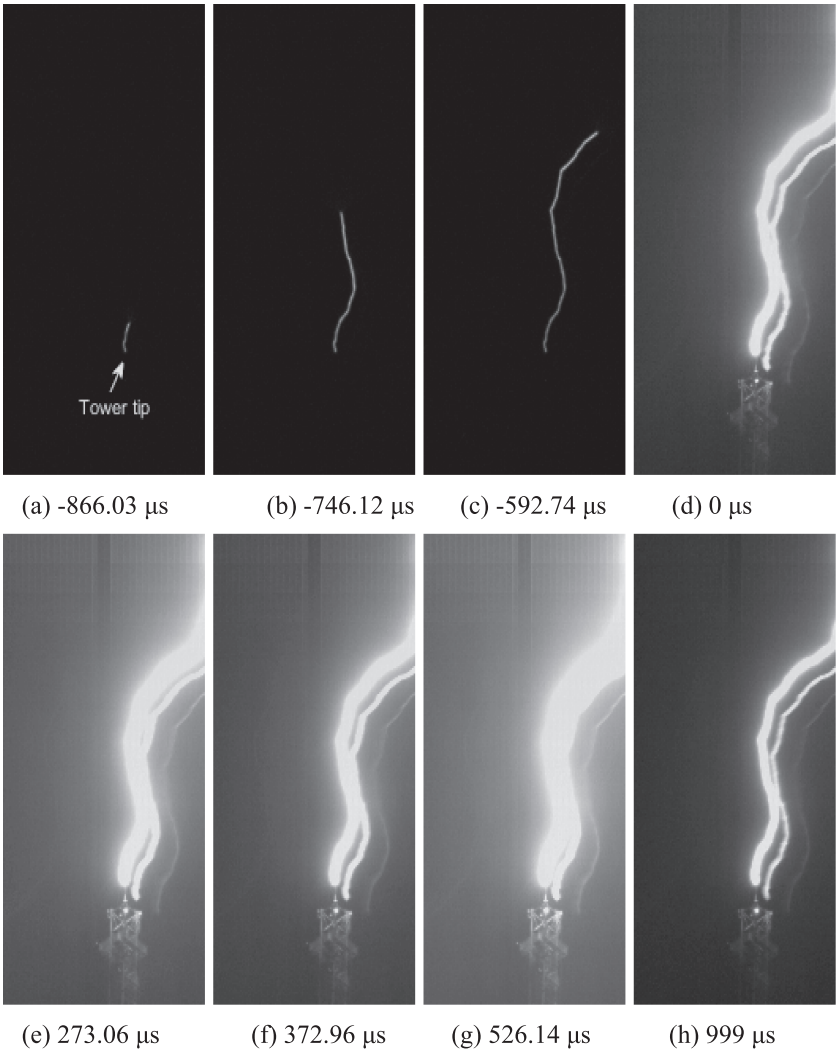

Figure 5. High-speed images for the initial upward positive leader (UPL2) and continuous current (ICC2) process for F1605, that is, IS2 in Figure 4. Panel (a) is the first frame the camera saw UPL2, (b)–(d) are three frames in the UPL2 stage, and (e)–(h) are four frames after UPL2 connected the cloud in the ICC2 stage. The weaker channel on the rightside of each panel in (d)–(h) is due to the window glass reflection in the observation room. The time here is the exposure time of each frame of the camera image.

of the continuous current process, or the sensor is at a remote distance to the current source. As will be seen in Figure 3, the channel light intensities for IS1, which more or less represent the channel currents, do show a 1.5- to 2-ms-long high light intensity (current) stage followed by a long low light intensity (current) tail (which is longer than 20 ms in the raw data). A similar long low light intensity (current) tail also exists for the RS process in this case. For this sake, the analysis of the magnetic field will be limited to the first 2-ms stage of IS1.

Figures 2 and 3 are the HC images and the channel luminous intensities for the initial stage IS1 in F1603, respectively. The captured RGB images were converted to grayscale images, and the grayscale intensity of each pixel in the images was then used to represent the channel luminous intensity. As can be seen from Figure 3, the channel luminous intensity showed an obvious stepwise property in the UPL1 stage and a periodical increasing and decreasing property in the ICC1 stage.

2.2.2. Case 2 (F1605)

F1605 occurred at 15:35:39, 30 July 2016, with its electric and magnetic field changes shown in Figure 4. Like F1603, the electric field changes in Figure 4 also show a nearby discharge that occurred about 82 ms before

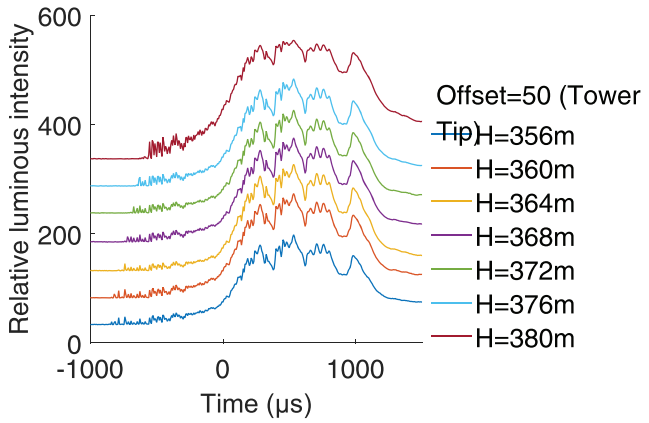

Figure 6. The relative luminous intensity versus time at seven different heights, plotted from the camera images for the initial upward positive leader (UPL2) and continuous current (ICC2) process for flash F1605, that is, IS2 in Figure 4. There is an offset of 50 between the curves for easy reading.

the start of F1605, indicating that F1605 was also an other-triggered type upward flash. F1605 included eight subprocesses, labeled as IS2 and RS1–RS7 in Figure 4, respectively. Among them, IS2 is used to designate the initial stage of F1605, which included a UPL2 process initiated at the tip of SZMGT and an ICC2 process. RS1–RS7 are seven downward leader-upward return-stroke sequences, which occurred at 654, 745, 786, 834, 842, 967, and 970 ms after IS2, respectively. Only the initial stage IS2 of F1605 will be analyzed in detail in the following sections. Similar to Case 1 the ringing distortion in magnetic field at the end of each of the IS2 and RS1–RS7 processes is due to the 80-Hz cutoff effect on the long continuous current tail after each of the events. Therefore, only the magnetic field corresponding to the first 2-ms stage of IS2 will be analyzed in detail.

Figures 5 and 6 are the HC images and the channel luminous intensities plotted from the camera images for the initial stage IS2 in F1605, respectively. The channel luminous intensities showed an obvious stepwise property in the UPL2 stage and a periodical increasing and decreasing property in the ICC2 stage.

3. Interpretation of Magnetic Fields in Initial Stage of Upward Flash

Figure 7 shows the enlarged magnetic fields for the initial stage of (a) F1603 and (b) F1605, respectively. As can be seen from the figure, both are characterized by a series of small fast-changing bipolar impulses superposed on a large slowly changing unipolar surge. The fast impulses have a time scale of about10 μs, while the slow surges have a time scale of about 2 ms. For good understanding of this property of the magnetic fields, in the following paragraphs, we use a simple model to simulate the magnetic fields produced by different current impulses along different leader channels over SZMGT.

As we know, the magnetic field measured for a lightning discharge is caused by the current propagating along the lightning channel. As shown in Figure 8, assuming there is a leader channel like C5 over SZMGT, for a perfect conductive ground condition, the horizontal magnetic field at B-sensor due to a current $i(t)$ along a channel segment (L1L2) can be calculated with equation (1) (Thottappillil & Rakov, 2001; Uman et al., 1975):

$$B_{\varnothing}(R,t)=\frac{1}{2\pi\varepsilon_0 c^2}\left[\int_{L1}^{L2}\frac{\sin\alpha(l)}{R^2(l)}i\left(l,t-\frac{R(l)}{c}\right)\mathrm{d}l+\int_{L1}^{L2}\frac{\sin\alpha(l)}{CR(l)}\frac{\partial i\left(l,t-\frac{R(l)}{c}\right)}{\partial t}\mathrm{d}l\right]. \quad (1)$$

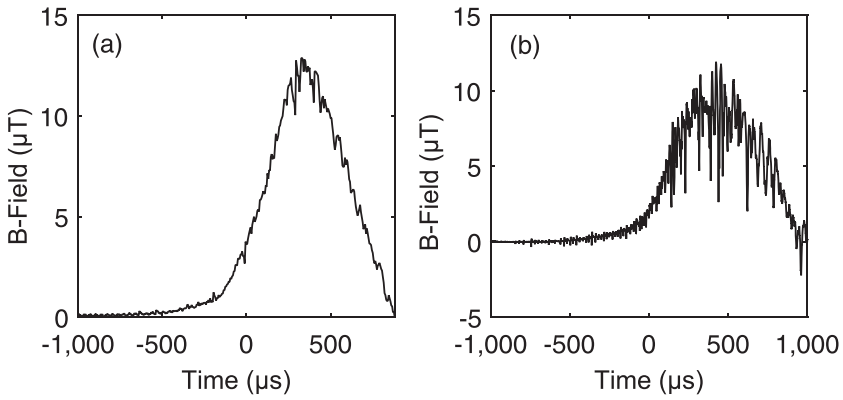

Figure 7. Measured magnetic fields for the initial stage of (a) F1603 and (b) Fl605.

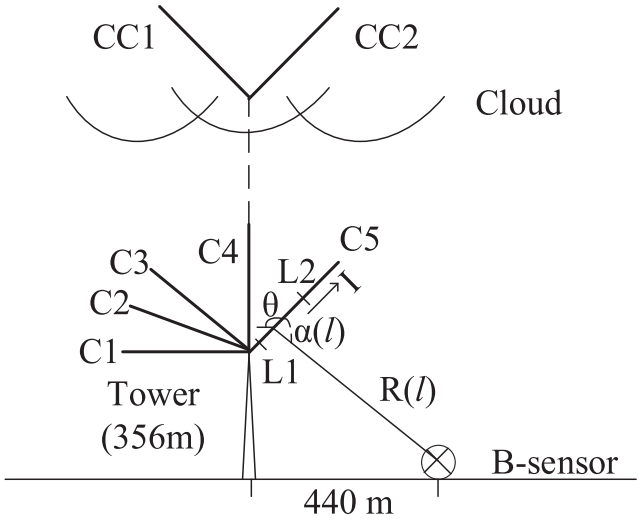

Figure 8. An illustration of the model for simulating the magnetic fields produced by currents along different leader channels over SZMGT above a perfect conductive ground plane. The length of all the five leader channels (C1–C5) connecting the tower and the two leader channels inside the cloud (CC1 and CC2) is assumed to be the same 356 m as the height of SZMGT. The elevation angles to the current propagation direction of C1 to C5 are 0°, 20°, 39°, 90°, and 135°, respectively, while that of CC1 and CC2 are 45° and 135°, respectively. The horizontal distance between the magnetic field sensor (B-sensor) and the tower base is 440 m. The elevation angle of the magnetic field sensor to the tower is about 39°, which is the same as the direction of C3. The magnetic field $B(t)$ at B-sensor due to a current $i(t)$ propagating along a segment L1L2 of a leader channel like C5 can then be estimated with equation (1).

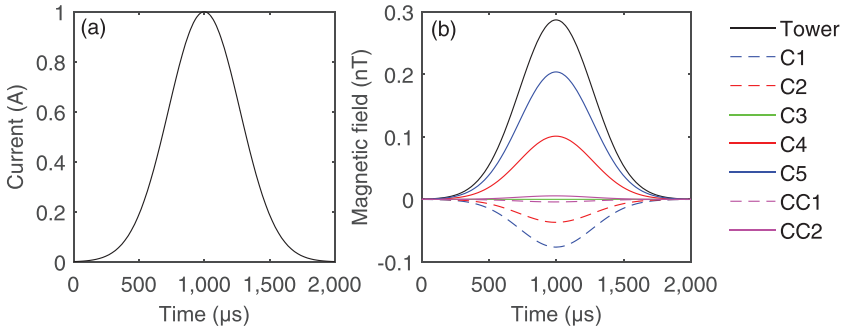

Figure 9. (a) A Gaussian waveform representing the slowly changing current of the initial stage of an upward flash. (b) The simulated magnetic fields caused by the current in (a) propagating along the tower and the seven different channels shown in Figure 8, respectively.

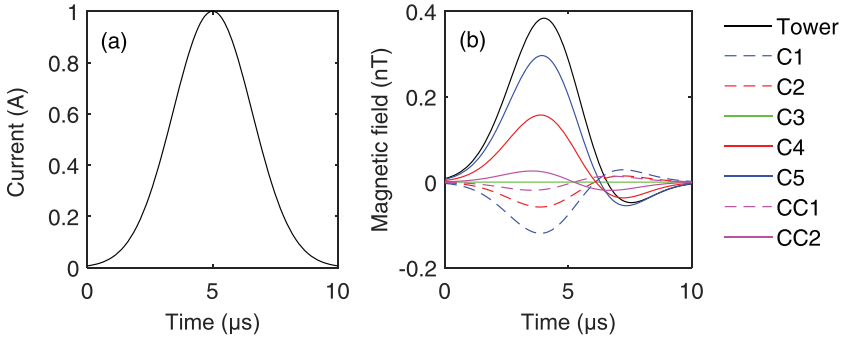

Figure 10. (a) A Gaussian waveform representing the fast-changing current component in the initial stage of an upward flash. (b) The results of simulated magnetic field impulses caused by the impulsive current propagating along the tower and the seven different channels shown in Figure 8, respectively.

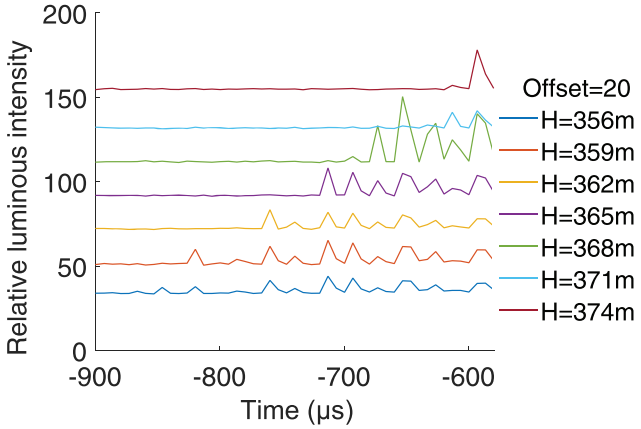

Figure 11. The channel relative luminous intensity versus time at seven different heights, for the 14 stepped processes of UPL1 observed in the field of view of the camera. There is an offset of 20 between the curves for easy reading.

In equation (1), the first and second terms on the rightside are the induction and radiation components of the magnetic field, respectively. It is customary to identify the induction component by its R^{-2} dependence and radiation component by its R^{-1} dependence. For the current, some previous studies showed that the

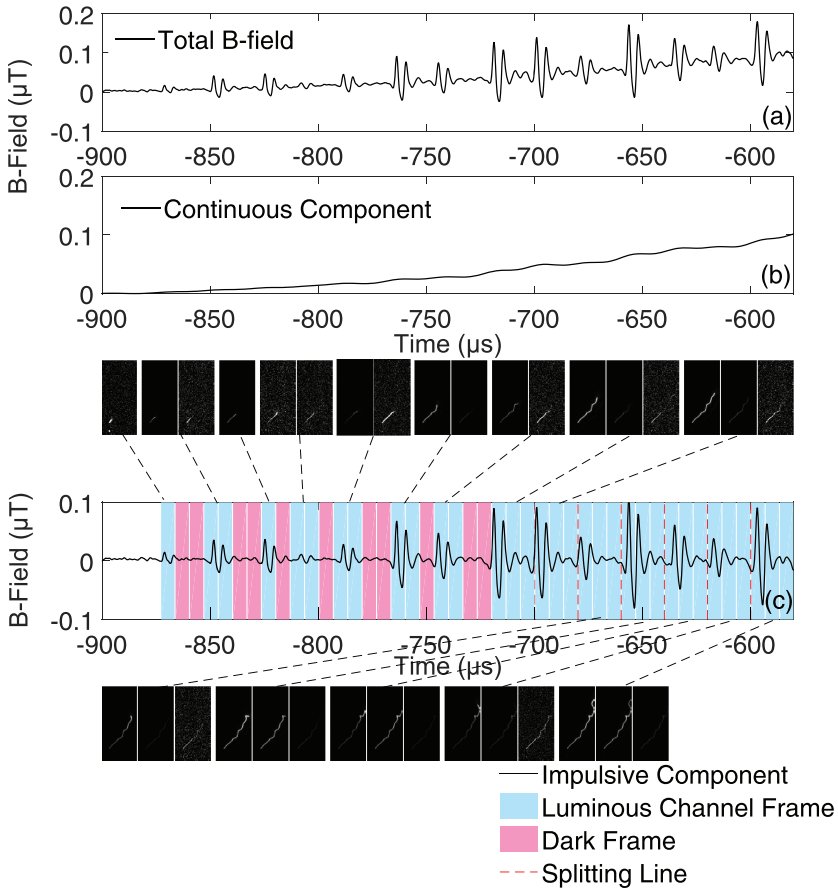

Figure 12. The magnetic fields for the 14 stepped processes of UPL1 observed in the field of view of the camera. Panel (a) is the total field, (b) the continuous component, and (c) the impulsive component. The blue and pink blocks in (c) represent the luminous and dark channel frames, respectively. Each camera frame has an exposure time of 6.18 μs and a dead time of 0.49 μs. Contrast enhancement was performed on some images for improved visualization.

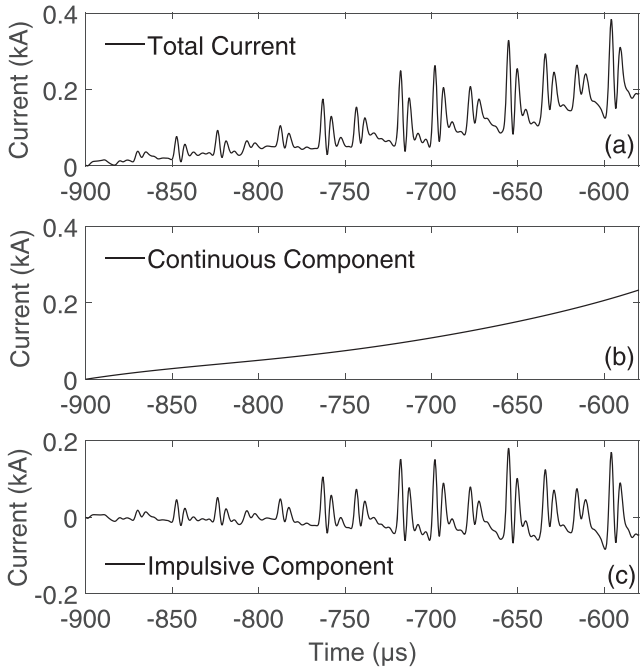

Figure 13. The current versus time retrieved from the magnetic fields for the 14 steps of UPL1 of F1603. Panel (a) is the total current, (b) the continuous component, and (c) the impulsive component.

initial stage of an upward discharge is usually characterized by several current impulses superimposed on a continuous current. The continuous current was assumed to be slowly changing and the same at all parts of the channel (Miki et al., 2006; Uman, 2001; Wang et al., 1999).

In this study, we focus on the polarity and variation trend of the magnetic field and current waveforms rather than their accurate values. Since the magnetic field and current impulses to be analyzed have a typical width of 10 μs, the current propagation time along a short channel segment (about 1 μs along a 300-m-long conductive channel) is small and has little influence on the magnetic field waveform. Therefore, for simplicity, we assume that both the impulsive and continuous currents are uniformly distributed along a short channel segment. Thus, equation (1) can be further simplified as follows:

Table 1
Information of the 14 Steps of UPL1 of F1603 Observed

Step no.	Step length (m)	Step extension time (μs)	Step extension speed (10^5 m/s)	Interstep interval (μs)	Average leader speed (10^5 m/s)
1	1.6	2.6	6.2	22.4	0.7
2	1.6	2.8	5.6	23.8	0.7
3	1.4	2.7	5.2	15.3	0.9
4	0.5	4.3	1.1	20.6	0.2
5	1.6	3.1	5.2	24.8	0.6
6	2.7	2.9	9.4	19.5	1.4
7	1.5	2.8	5.2	25.1	0.6
8	2.2	3.3	6.8	20.3	1.1
9	2.2	2.8	7.9	20.1	1.1
10	1.2	3.2	3.9	22	0.5
11	0.6	3.2	2	20.8	0.3
12	2.0	3.8	5.4	18.8	1.1
13	2.4	3.3	7.4	19.9	1.2
14	2.4	3.3	7.3		
Min	0.5	2.6	1.1	15.3	0.2
Max	2.7	4.3	9.4	25.1	1.4
Mean	1.7	3.2	5.6	21	0.8

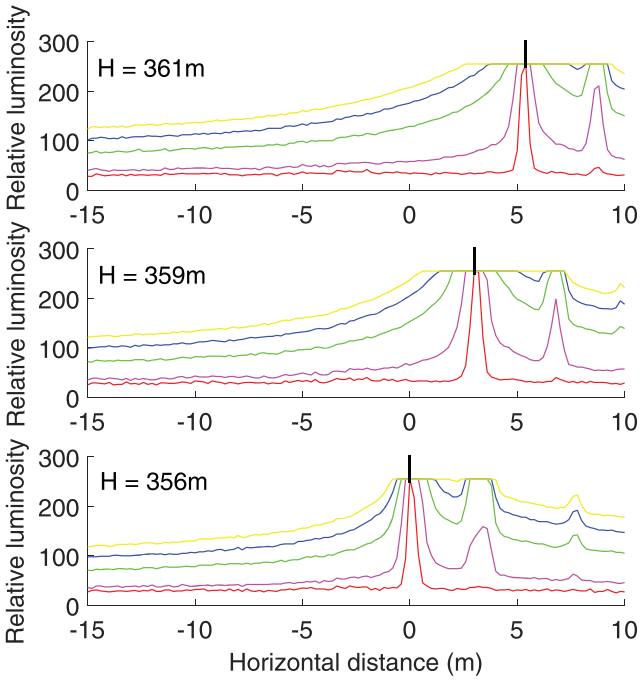

Figure 14. The relative luminosity versus horizontal distance at different heights (the lower, middle, and upper panels are for the heights of 356, 359, and 362 m, respectively) and at different times in the initial stage of F1603. The red (−300.18 μs) and pink (6.18 μs) curves are for the UPL1 stage, and the blue (252.6 μs), green (285.9 μs), and yellow (332.52 μs) ones are for the ICC1 stage. The black vertical bar is used to designate the center of the channel core.

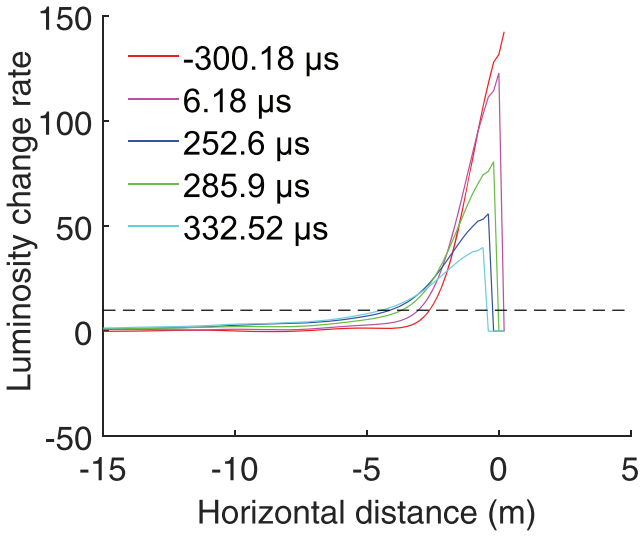

Figure 15. The luminosity spatial change rate versus horizontal distance at the height 356 m at different times for the initial stage of F1603. The black dashed line represents the critical value for defining the left edge of the luminous channel of F1603 at a certain height and time.

$$B_{\varnothing}\left(t+\frac{R}{c}\right)=\frac{l\sin\alpha}{2\pi\varepsilon_0 c^2 R}\left[\frac{1}{R}i(t)+\frac{1}{C}\frac{\partial i(t)}{\partial t}\right], \quad (2)$$

where l is the length of channel segment L1L2 and R and sinα are the average distance and direction factor of the segment L1L2 to the magnetic field sensor. Equation (2) is a typical differential problem that can be easily solved.

To analyze the characteristics of magnetic field waveforms obtained for the initial stages of the two flashes shown in Figure 7, some simulation works based on Figure 8 and equation (2) have been done. In the simulation, the tower is set to 356 m high and the cloud is 3 km high. Suppose there are five different upward leader channels initiated from the top of the tower (C1–C5) and two different leader channels in the cloud (CC1 and CC2) with different current directions, as shown in Figure 8, all these seven leader channels are set to the same 356 m long as the height of the tower. The elevation angles from the horizon to the current direction for C1 to C5 are 0°, 20°, 39°, 90°, and 135°, respectively, and that for CC1 and CC2 are 45° and 135°, respectively.

3.1. Continuous Component of the Magnetic Field

The Gaussian waveform shown in Figure 9a, which has a waveform width of 2 ms, is used to represent the continuous component (slowly changing) in the initial stage of an upward flash. Shown in Figure 9b are the results of simulated magnetic fields caused by the continuous current along the tower and the seven different channels (C1–C5, CC1, and CC2). The results show that the magnetic fields caused by the continuous current along the tower (black solid line), C4 (red solid line), C5 (blue solid line), and CC2 (pink solid line) have the same positive polarity but that by C1 (blue dashed line), C2 (red dashed line), and CC1 (pink dashed line) have the same negative polarity and that by C3 (green solid line) is 0. The reason for these differences is due to that the polarity of the magnetic field is determined by the sinα in equation (2), which for C4, C5, CC2, and the tower is positive but for C1, C2, and CC1 is negative and for C3 is just 0.

According to the simulation results, the continuous current along the tower has the largest influence on the simulated magnetic field. No matter what elevation angle of the leader channel is, the magnetic field caused by the continuous current is dominated by the inductive field component from the tower body rather than the leader channel in free air above the tower or inside the cloud, which is consistent with some previous researches (Kordi et al., 2003; Rachidi et al., 2001).

3.2. Impulsive Component of the Magnetic Field

In addition, to simulate the fast-changing magnetic field impulses caused by the impulsive current component, the Gaussian waveform shown in Figure 10a is used as the impulsive current, which has a waveform width of 10 μs. The magnetic impulses caused by the impulsive current along the tower and the seven leader channels (C1–C5, CC1, and CC2) are calculated, as shown in Figure 10b. There are two points that can be drawn from the simulated magnetic impulses. The first point is that while the current impulse has a unipolar waveform, it produces a bipolar magnetic field impulse, no matter which channel the current impulse propagates along. This means

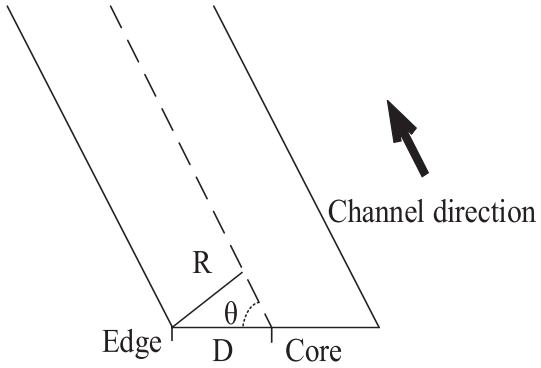

Figure 16. Illustration for the luminous channel radius estimation. D represents the horizontal distance from the edge to the core of the channel, and R represents the luminous channel radius.

that such an impulsive magnetic field is dominated by the radiation component rather than the inductive one. The second point is that the first peak polarity of the bipolar magnetic impulse caused by the tower, C4, C5, and CC2, is the same positive, while that caused by C1, C2, and CC1 is the same negative. The reason for this point is due to the sign of $sin\alpha$ in equation (2), the same reason for that of the slowly changing case.

4. Channel Evolution in Initial Stage of Upward Flash

4.1. Case 1: F1603

4.1.1. Stepwise Property of UPL1

The initial stage of F1603 consists of the UPL1 and the continuous current (ICC1) processes. Both the camera images and the magnetic fields show that UPL1 had obvious stepwise characteristics. There are 14 stepped processes of UPL1 captured in the field of view of the camera, which the step length is estimated to range from 0.5 to 2.7 m with a mean of 1.7 m.

Shown in Figures 11 and 12 are the relative channel luminous intensity versus time and height and the magnetic fields with corresponding camera images, respectively, for the 14 stepped processes of UPL1 observed. Comparing the magnetic fields with the channel luminous intensities, we find that each stepped process produced a bipolar magnetic impulse whose polarity of the first peak was positive. According to the simulations in section 3.2, this kind of magnetic impulses should be due to current impulses flowing along a channel like C4 or C5, for which the $sin\alpha$ is positive.

As shown by equation (2), knowing the magnetic field waveform and the lightning channel position, the current waveform along the channel can be easily obtained. For better understanding of UPL1, a typical iterative method for solving differential problem is used in equation (2) to retrieve the current along the leader channel from the magnetic fields shown in Figure 12.

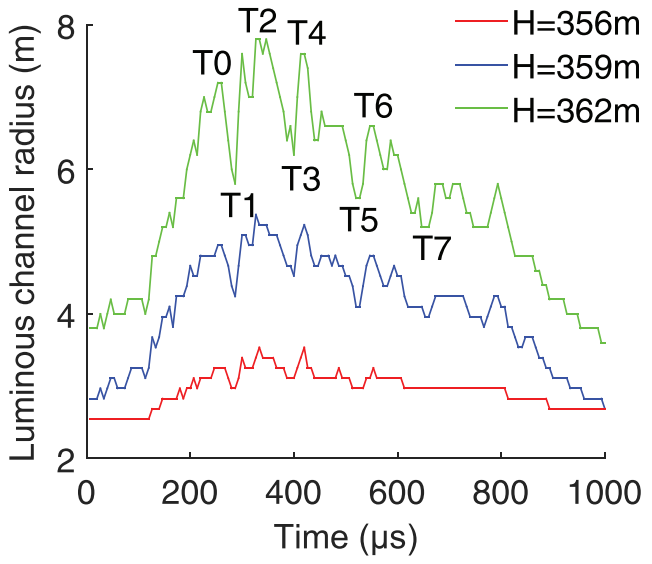

Figure 17. The radius of luminous channel versus time at different heights (356, 359, and 362 m) for the initial stage of F1603. The T_0 (252.6 μs), T_2 (332.52 μs), T_4 (419.1 μs), and T_6 (552.3 μs) are used to designate four peak value times during channel expansions, and T_1 (285.9 μs), T_3 (399.12 μs), T_5 (525.66 μs), and T_7 (625.56 μs) are used to designate four valley value times during channel shrinkages.

For the continuous component, simulations in section 3.1 show that the current along the tower has the largest influence on the magnetic field. Therefore, only the tower was considered in retrieving the continuous current component. For the impulsive component, it is generally thought that the impulsive current due to a stepped process is generated at the tip of the leader channel and propagates backward along the leader channel with dramatic attenuations (Chen et al., 1999; Wang et al., 2016). This means that the impulsive current along the stepped leader channel has the largest influence on the impulsive component of the *B* field observed. Therefore, only a short channel segment from the tower tip up to the stepped leader tip at the moment was considered in retrieving the impulsive currents. Besides, it is noted that the 14 magnetic field impulses of UPL1 have a similar positive polarity to that of the simulated magnetic impulses in section 3.2 for channels C4 and C5, for which the channel direction factor $sin\alpha$ is positive. Since we just have the 2-D image for UPL1, we do not know the exact channel direction and length that is with the impulsive current. So we take a 10-m-long channel segment above the tower tip with a channel direction factor $sin\alpha = +1$ for retrieving the impulsive current from the magnetic field with equation (2). With such an assumption, the polarity and variation trend of the retrieved impulsive current would be largely correct, but its amplitude would be with a big error and is just for reference. Since the magnetic field is cut off at 80 Hz, the retrieved continuous current might be underestimated if it contains rich components below 80 Hz.

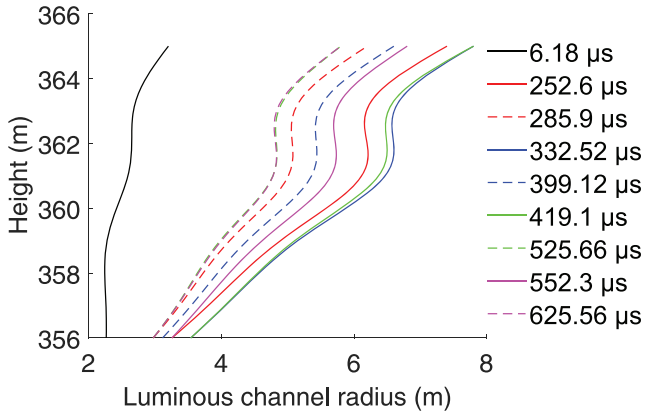

Figure 18. The radius of luminous channel versus height at different times for the initial stage of F1603. The original radius data are smoothed with the 5-point smoothing technique. The black line (6.18 μs) is for the UPL1 stage and others for the ICC1 stage. Dashed lines are for the valley values during channel shrinkages (T_1: 285.9 μs, T_3: 399.12 μs, T_5: 525.66 μs, and T_7: 625.56 μs), and solid lines are for the peak values during channel expansions (T_0: 252.6 μs, T_2: 332.52 μs, T_4: 419.1 μs, and T_6: 552.3 μs).

Shown in Figure 13 are the retrieved currents from the magnetic fields for UPL1. The continuous current increases smoothly as UPL1 extends upward, while the impulsive current has an oscillatory shape. The oscillation of the current may be due to the transient process excited in the tower. These are consistent with some previous current pulses recorded in the rocket-triggered lightning (Lalande et al., 1998).

If we assume the rising time of the first current pulse in each stepped process as the extension time of each step, the 2-D extension speed of each step of UPL1 can be estimated from the step length and extension time. The estimate of the step extension time ranges from 2.6 to 4.3 μs with a mean value of 3.2 μs and that of the step extension speed ranges from 1.1 to 9.4 × 10^5 m/s with a mean value of 5.6 × 10^5 m/s. The interstep interval ranges from 15.3 to 25.1 μs with a mean value of 21 μs, and the average leader speed is estimated in the range of 0.2–1.4 × 10^5 m/s with a mean value of 0.8 × 10^5 m/s. Details of the 14 leader steps are listed in Table 1.

4.1.2. Channel Expansion Property of ICC1

To analyze the expansion and shrinkage property of luminous channels, luminosities of all pixels in each frame of each HC image in the ICC1 stage of F1603 were examined. Shown in Figure 14 are the relative luminosity versus horizontal distance (horizontal pixel) in a frame of camera image at different heights (the lower, middle, and upper panels are for the heights of 356, 359, and 362 m, respectively) and at different times (the red, pink, blue, green, and yellow curves in each panel are for the times of −300.18, 6.18, 252.6, 285.9, and 332.52 μs, respectively). Among them, the red (−300.18 μs) and pink (6.18 μs) curves present the luminosities of the channel in the UPL1 stage of which the peak value point can be seen as the center of UPL1 channel core. The others (blue, green, and yellow) present the channel luminosities in the ICC1 stage. There are more than one luminosity peaks in each curve in the Figure of which the left one is corresponding to the true channel and the right ones are due to window glass reflections.

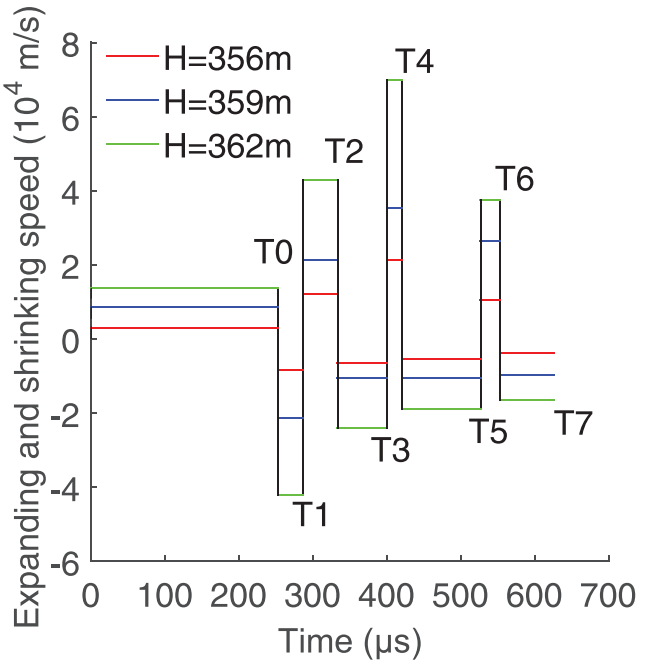

Figure 19. The channel expanding and shrinking speeds versus time at different heights for the initial stage of F1603. Positive values mean expansions and negative values mean shrinkage. T_0–T_7 are eight time points defined in Figure 17.

To estimate the radius of the luminous channel, the part of each luminosity curve left to the core center (Figure 14) is further processed to get the luminosity spatial change rate versus horizontal distance at different times and heights, as shown in Figure 15. The left edge of the luminous channel is then defined as the first pixel from the left whose luminosity change rate is larger than a critical value, say 10, as shown by the dashed horizontal line in Figure 15. Thus, the horizontal distance (D) between the edge and the core center of the luminous channel at a certain height and time can be estimated. As shown in Figure 16, the luminous channel radius (R) is estimated by $R = D \times \sin(\theta)$, where θ is the angle between the luminous channel direction and the horizontal direction.

The radius of the luminous channel for the initial stage of F1603 as a function of the time at different heights (Figure 17) and as a function of the height at different times (Figure 18) has been estimated.

As can be seen in Figure 17, the temporal evolution of the luminous channel radius at a given height shows a general expansion trend before the time $T_0 = 252$ μs. After that, it shows a periodical shrinking and expanding trend, as indicated in Figure 17 by the peaks at times T_0, T_2, T_4, and T_6 and the valley values at times T_1, T_3, T_5, and T_7. The maximum value of the luminous channel radius appears at T_2 =

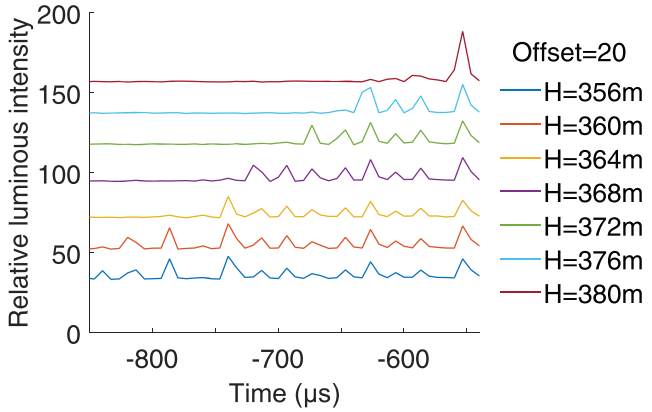

Figure 20. The relative channel luminous intensity of the 13 stepped processes versus time at seven different heights for UPL2 of F1605. There is an offset of 20 between curves for easy reading.

332.52 μs. Such a channel expansion and shrinkage property is well corresponding to the magnetic field fluctuations in Figure 7a for F1603.

As can be seen in Figure 18, the channel radius shows an obvious increasing trend with the increase of height at a given time. At the UPL1 stage (black line, 6.18 μs), the channel radius is about 2.5 m at 356 m high (the tower tip) and 4 m at 365 m high (9 m above the tower tip). When come to the mature stage of ICC1, the channel radius fluctuates against time in the range of 2.9–3.5 m when at 356 m high and of 5.8–7.8 m when at 365 m high.

Based on the change rate of channel radius versus time, the channel expanding speeds for the time intervals of 0–T_0, T_1–T_2, T_3–T_4, and T_5–T_6 and the channel shrinking speeds for the time intervals of T_0–T_1, T_2–T_3, T_4–T_5, and T_6–T_7 are estimated, as shown in Figure 19, where the positive value stands for expansion and the negative one for shrinkage. The majority of the expanding and shrinking speeds are of 10^4 m/s, and the maximum channel expanding speed is about 7.0×10^4 m/s.

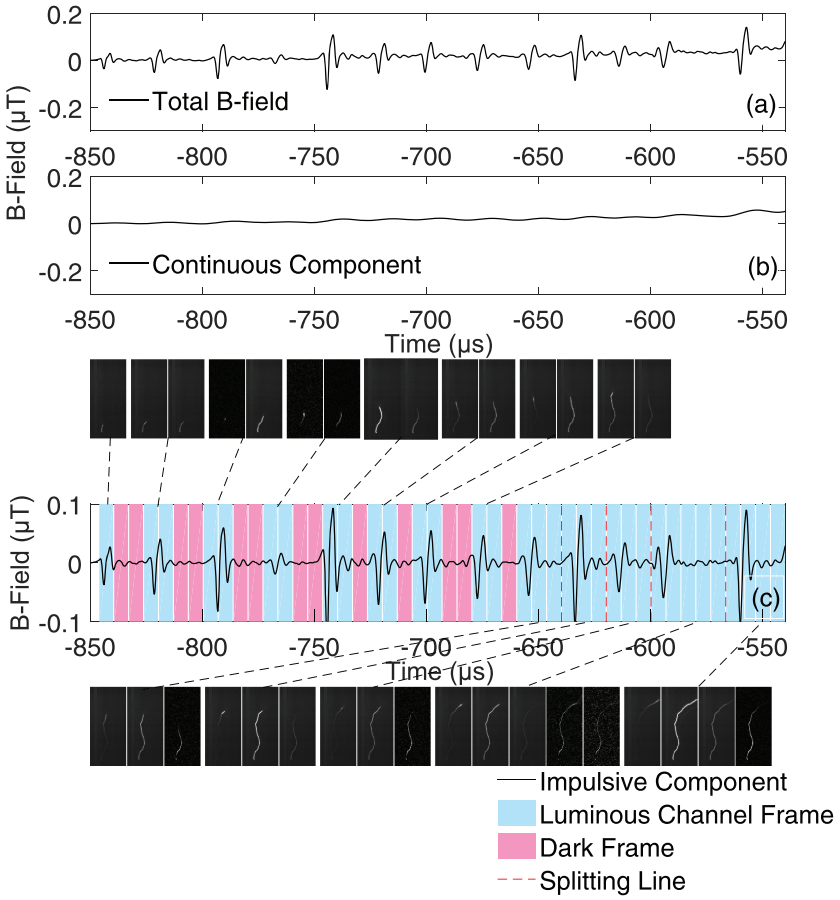

Figure 21. Magnetic fields of the 13 stepped processes and the corresponding images captured by the camera for F1605: (a) the total magnetic field, (b) the continuous component, and (c) the impulsive component. The blue and pink blocks in (c) represent the luminous and dark frames of the channel images, respectively. Each frame has an exposure time of is 6.18 μs and dead time of 0.49 μs. Contrast enhancement was performed on some images for improved visualization.

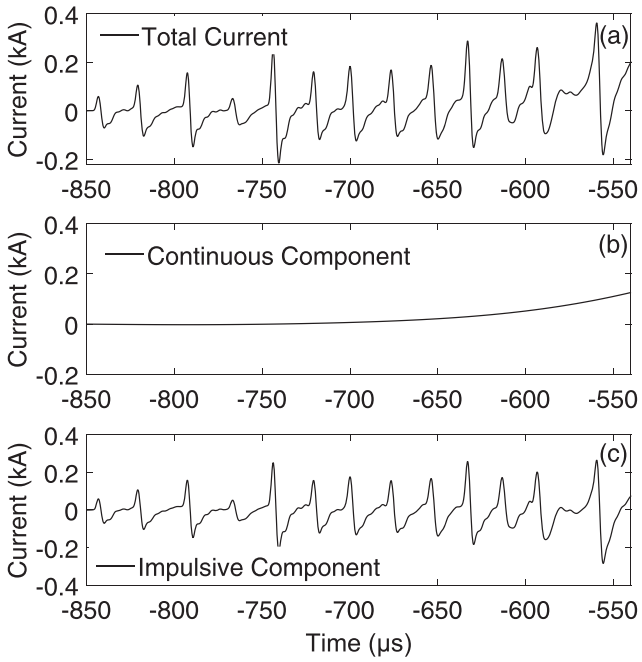

Figure 22. The estimated current versus time for UPL2 in F1605. (a) The total current, (b) the continuous component, and (c) the impulsive component.

4.2. Case 2: F1605

4.2.1. Stepwise Property of UPL2

Like Case 1, both the camera images and the magnetic fields show that UPL2 of F1605 had obvious stepwise characteristics. There are 13 stepped processes of UPL2 viewed by the camera, which the step length is estimated to range from 1.2 to 3 m with a mean of 2.2 m.

Shown in Figures 20 and 21 are the relative channel luminous intensity versus time at different heights and the magnetic field changes with corresponding camera images, respectively, for the 13 stepped processes of UPL2 viewed by the camera. As can be seen in these figures, each stepped process produced a bipolar magnetic impulse whose polarity of the first peak was negative. Based on the simulations on impulsive currents in section 3.2, this kind of magnetic impulse might be due to a current impulse along a leader channel that is inclined away from the magnetic sensor like channels C1 and C2, for which the direction factor $\sin\alpha$ is negative.

Like Case 1, the current for UPL2 in Case 2 is retrieved from the magnetic fields. For the continuous component, only the tower is considered for retrieving the current. For the impulsive component, a 10-m-long channel segment from the tower tip up with a channel direction factor $\sin\alpha = -1$ was taken for retrieving the impulsive current from the magnetic field with equation (2). With this assumption, the polarity and variation trend of the retrieved current would be largely correct, but its amplitude would be with a big error and is just for reference. The retrieved current for UPL2 is shown in Figure 22. As can be seen in Figure 22, the continuous current increases smoothly as UPL2 extends upward, while the impulsive current is oscillatory. Since the magnetic fields are cut off at 80 Hz, the continuous current value might be underestimated if it contains rich components below 80 Hz.

Assuming that the rising time of the first peak of each current impulse is the extension time of each step, the extension speed of each step for UPL2 can be estimated. The estimate of step extension time ranges from 3 to 7 μs with a mean value of 4.3 μs and that of step extension speed ranges from 2.2 to 9.2×10^5 m/s with a mean value of 5.4×10^5 m/s. The interstep interval ranges from 19.3 to 30 μs with a mean value of 23.4 μs, and the

Table 2
Detailed Information of the 13 Steps of UPL2 of F1605 Observed

Step no.	Step length (m)	Step extension time (μs)	Step extension speed (10^5 m/s)	Interstep interval (μs)	Average leader speed (10^5 m/s)
1	2.2	3.8	5.7	20.8	1
2	1.2	5.4	2.2	29.2	0.4
3	1.6	4.4	3.7	25.2	0.6
4	3	5.2	5.8	22.8	1.3
5	1.5	5.3	2.8	25.2	0.6
6	2.9	3.2	9.2	19.3	1.5
7	2.2	4.5	4.8	24.7	0.9
8	2.2	3.3	6.6	22.3	1
9	2.3	3.8	6.1	20.5	1.1
10	2.4	4	5.9	20.2	1.2
11	2.5	3.5	7.3	20.4	1.2
12	2.4	3	7.9	30	0.8
13	1.9	7	2.7		
Min	1.2	3	2.2	19.3	0.4
Max	3	7	9.2	30	1.5
Mean	2.2	4.3	5.4	23.4	1.0

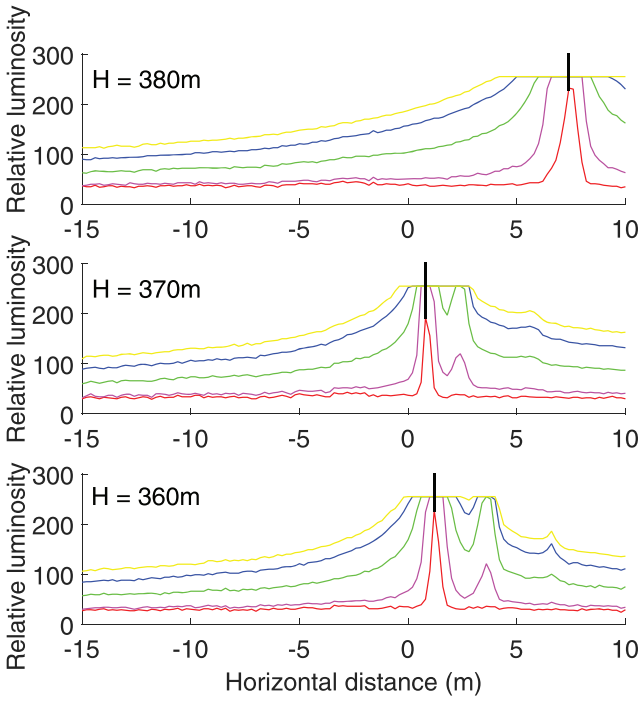

Figure 23. The relative luminosity versus horizontal distance at three different heights (360, 370, and 380 m, respectively) and at five different times for the initial stage of F1605. The red (−300.18 μs) and pink (6.18 μs) curves are for the UPL2 stage, and the blue (279.24 μs), green (379.14 μs), and yellow (532.32 μs) are for the ICC2 stage of F1605. Black vertical bar is used to designate the center of the channel core.

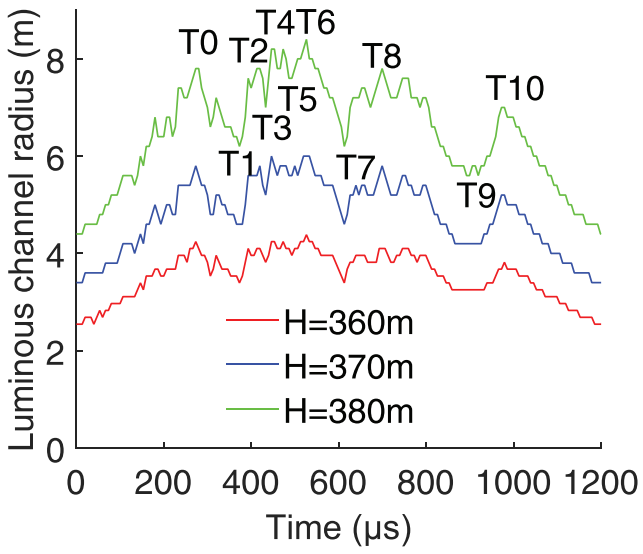

Figure 24. The radius of luminous channel versus time at three different heights (360, 370, 380 m, respectively) for the initial stage of F1605. The T_0 (279.24 μs), T_2 (425.76 μs), T_4 (452.4 μs), T_6 (532.32 μs), T_8 (705.48 μs), and T_{10} (985.2 μs) refer to six radius peak value times during channel expansions, while T_1 (379.14 μs), T_3 (439.08 μs), T_5 (499.02 μs), T_7 (618.9 μs), and T_9 (898.62 μs) refer to five radius valley value times during channel shrinkages.

average leader speed of UPL2 ranges from 0.4 to 1.5×10^5 m/s with a mean value of 1.0×10^5 m/s. Details of the 13 steps are listed in Table 2.

4.2.2. Channel Expansion Property of ICC2

With the same method for Case 1, luminosities of all pixels in each camera image against the time are examined to find the evolution of luminous channel radius of ICC2 in F1605. Shown in Figure 23 are the curves of the relative luminosity versus horizontal distance in each image at three different heights (360, 370, and 380 m, respectively) and at five different times (−300.18, 6.18, 279.24, 379.14, and 532.32 μs, respectively). The red and pink curves present the luminosities of the channel in the UPL2 stage, of which the peak value point can be seen as the center of the UPL2 channel core. The others (blue, green, and yellow) present the luminosities of the channel during the ICC2 stage. There are more than one luminosity peaks in each curve, of which the left one is corresponding to the true channel and the right ones are due to window reflections.

Like Case 1, the radius of luminous channels of ICC2 of F1605 as a function of the time at different heights (Figure 24) and as a function of the height at different times (Figure 25) is obtained.

As can be seen in Figure 24, the temporal evolution of the luminous channel radius at a given height, from the UPL2 stage to the mature stage of ICC2, shows a general expansion trend. When come to the mature stage of ICC2, it shows a periodical shrinking and expanding trend, as indicated by the peak values at times T_0, T_2, T_4, T_6, T_8, and T_{10} and the valley values at times T_1, T_3, T_5, T_7, and T_9 in Figure 24. Such a channel radius expansion and shrinkage property is consistent with the fluctuation property of magnetic fields of the initial stage of F1605 shown in Figure 7b.

As can be seen in Figure 25, the luminous channel radius shows an obvious increasing trend with the increase of height at a given time. In the UPL2 stage (black line, 6.18 μs), the radius is about 2.5 m at 356 m high (the tower tip) and 4.4 m at 380 m high (24 m above the tower tip). When in the ICC2 stage, the radius fluctuates against time in the range of 2.8–3.5 m when at 356 m high and of 5.6–8.4 m when at 380 m high.

Similar to Case 1, the channel expanding speeds for the time intervals of 0–T_0, T_1–T_2, T_3–T_4, T_5–T_6, T_7–T_8, and T_9–T_{10} and the channel shrinking speeds for the time intervals of T_0–T_1, T_2–T_3, T_4–T_5, T_6–T_7, and T_8–T_9 at different heights and times, for ICC2 of F1605, are estimated. The results are shown in Figure 26, where positive values represent channel expansions and negative values represent channel shrinkages. The majority of the channel expansion and shrinkage speeds are of 10^4 m/s, and the maximum channel expansion speed is about 9.0×10^4 m/s.

5. Conclusion and Discussion

In this paper, we have analyzed the initial stages of two upward negative flashes (F1603 and F1605) initiated at the tip of the 356-m SZMGT, at 15:23:22 and 15:35:39, 30 July 2016, respectively. For both flashes, the initial stage consisted of a UPL process followed by an

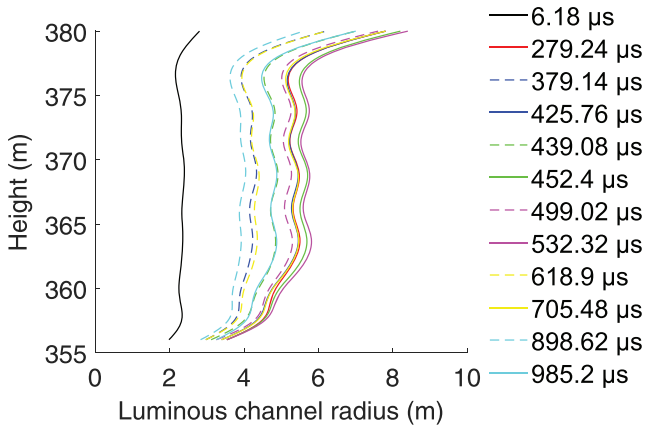

Figure 25. The radius of luminous channel versus height at different times for the initial stage of F1605. The original radius data were smoothed with the 5-point smoothing technique. The black line (6.18 μs) is for the UPL2 stage and the others for the ICC2 stage. The dashed lines refer to the radius valley values during channel shrinkages at T_1: 379.14 μs, T_3: 439.08 μs, T_5: 499.02 μs, T_7: 618.9 μs, and T_9: 898.62 μs, respectively, while the solid lines refer to the radius peak values during channel expansions at T_0: 279.24 μs, T_2: 425.76 μs, T_4: 452.4 μs, T_6: 532.32 μs, T_8: 705.48 μs, and T_{10}: 985.2 μs, respectively.

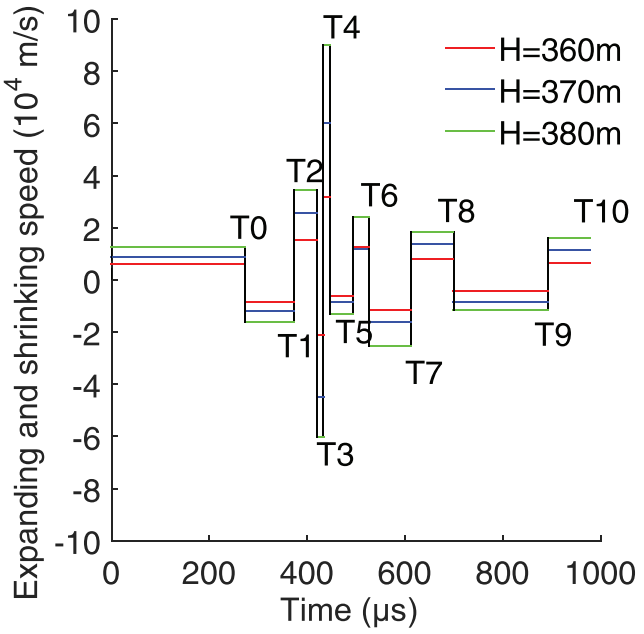

Figure 26. The channel expanding and shrinking speeds versus time at three different heights during the ICC2 stage of F1605. Positive value means expansion, and negative value means shrinkage. T_0–T_{10} are the 11 time points defined in Figure 24.

ICC process. The data analyzed included the magnetic field measurements and HC images. Besides, based on the magnetic field measurements, the relative leader currents were also estimated with a simplified model for better understanding of the leader behavior. The major results are summarized and discussed as follows:

1. The magnetic fields associated with the initial stage of the two flashes were found to be consisted of two components: a slowly changing continuous component and a series of fast-changing impulsive component superposed on the continuous component. The continuous component first showed a continuous increasing trend during the UPL stage, then a fluctuating and finally a continuous decreasing trend after the UPL contacted the cloud during the ICC stage. We infer that such a slowly changing continuous component is due to a continuous current along the leader channel and the tower. According to the simulation results, the continuous current along the tower has the most significant influence on the magnetic field measurements.
2. The impulsive magnetic fields associated with the initial UPL of the two flashes were found to be bipolar ones, but the polarity of the first peak of each bipolar impulse in two cases was opposite. Each magnetic field impulse was found to be associated with a stepped leader process observed by the HC, produced by a current impulse that might start at the leader tip by a step process and propagate backward (downward). According to simulations, the positive polarity of the first peak of each bipolar magnetic impulse for UPL1 means that the UPL1 channel might be inclined in the direction close to the B-sensor. The negative polarity of the first peak of each bipolar impulse for UPL2 means that the UPL2 channel might be inclined in the direction away from the B-sensor.
3. There are 14 and 13 stepped processes in the initial UPL stages for F1603 and F1605, respectively, which were captured in the field of view of the HC. Each leader stepped process was corresponding to a magnetic field impulse. Leader step parameters estimated include the following: (a) The step length, ranging from 0.5–2.7 m with a mean of 1.7 m for F1603 and from 1.2–3 m with a mean of 2.2 m for F1605. (b) The interstep interval, ranging from 15.3–25.1 μs with a mean value of 21 μs for F1603 and from 19.3–30 μs with a mean value of 23.4 μs for F1605. (c) The average 2-D leader speed, ranging from 0.2–1.4 × 10^5 m/s with a mean value of 0.8 × 10^5 m/s for F1603 and from 0.4–1.5 × 10^5 m/s with a mean value of 1.0 × 10^5 m/s for F1605. (d) By assuming the initial rising time of the current impulse of each stepped process as the step extension time, each step extension speed was estimated. The estimated step extension speed ranged from 1.1–9.5 × 10^5 m/s with a mean value of 5.6 × 10^5 m/s for F1603 and from 2.2–9.2 × 10^5 m/s with a mean value of 5.4 × 10^5 m/s for F1605. We though that the front rising time of a step current impulse is closely related to the breakthrough time of the step length. This is just an assumption with no solid physical ground.
4. The channel luminosity and luminous channel radius for the initial stages of the two flashes as a function of time and height were obtained and analyzed. The channel luminosity showed a general increasing trend with time when in the UPL stage but a periodical brightening and weakening process in an interval time of about tens of microsecond when in the ICC stage. Such a

periodical brightening and weakening process was well consistent with magnetic field pulses during the ICC stage. The luminous channel radius at any a given height showed a general increasing trend (increases from about 2 m to about 10 m) with time when in the UPL stage but a periodical shrinking and expanding process (between 6 and 10 m in an interval of tens of microsecond) when in the ICC stage. The majority of channel expanding and shrinking speeds were the order of 10^4 m/s with the maximum channel expanding speed being about 9.0×10^4 m/s. These results are well consistent with the theoretical predictions on corona sheath by Maslowski and Rakov (2006), who first calculated the corona sheath radius of lightning channel as several meters and the channel expanding speed as 10^4–10^5 m/s.

5. Particularly, the luminous channel radius showed an increasing trend with the increase of height at any a given time. For example, when in the UPL stage, the luminous channel radius was about 2 m around the tower tip and about 4 m at 9 m high above the tower tip. When in the ICC stage, the channel radius was about 3 m around the tower tip and about 10 m at 9 m high above the tower tip. Such a feature of the luminous channel is well consistent with the concept of leader corona sheath model for a UPL in literature. We infer that the ICC process is that negative charges flow from the cloud downward to neutralize positive charges deposited in the corona sheath during the UPL stage. The maximum luminous channel radius in the ICC stage may be a good indicator of the corona sheath radius of the UPL stage. The periodical channel shrinking and expanding phenomena might be due to some newly developed in-cloud leader/streamer branches attaching to the main channel during the ICC stage. Lateral discharges within corona sheath causing broadening of the optical channel of lightning were also reported by Takagi et al. (1998).

Acknowledgments
Works leading to this paper are funded by the Research Grants Council of Hong Kong Government (Grants: PolyU 152652/16E and PolyU 152147/19E). Data used in this paper can be accessed online (http://doi.org/10.5281/zenodo.3370222).

References

Arima, I., Watanbe, T., Takagi, N., & Kakihara, M. (1998). Experimental study of the corona current in lightning return stroke, paper presented at 9th International Conference on Gas Discharge and their Application. Venice, Italy.

Berger, K. (1978). Blitzstorm-Parameter von Aufwartsblitzen. *Bulletin of Schweizerischer Electrotechnische*, *69*, 353–360.

Biagi, C. J., Uman, M., Hill, J., & Jordan, D. (2011). Observations of the initial, upward-propagating, positive leader steps in a rocket-and-wire triggered lightning discharge. *Geophysical Research Letters*, *38*, L24809. https://doi.org/10.1029/2011GL049944

Cabrera, V. M., & Cooray, V. (1992). On the mechanism of space charge generation and neutralization in a coaxial cylindrical configuration in air. *Journal of Electrostatics*, *28*(2), 187–196. https://doi.org/10.1016/0304-3886(92)90070-A

Chan, M.-K., Chen, M., & Du, Y.-p. (2018). A macroscopic physical model for self-initiated upward leaders from tall grounded objects and its application. *Atmospheric Research*, *200*, 13–24. https://doi.org/10.1016/j.atmosres.2017.09.012

Chen, L., Lyu, W., Zhang, Y., Ma, Y., Qi, Q., Wu, B., & Zhu, Y. (2019). Correlated luminosity and magnetic field peaks produced by canton tower-strokes. *Atmospheric Research*, *218*, 59–69. https://doi.org/10.1016/j.atmosres.2018.11.008

Chen, M., Takagi, N., Watanabe, T., Wang, D., Kawasaki, Z. I., & Liu, X. (1999). Spatial and temporal properties of optical radiation produced by stepped leaders. *Journal of Geophysical Research*, *104*(D22), 27,573–27,584. https://doi.org/10.1029/1999JD900846

Diendorfer, G., Pichler, H., & Mair, M. (2009). Some parameters of negative upward-initiated lightning to the Gaisberg tower (2000–2007). *IEEE Transactions on Electromagnetic Compatibility*, *51*(3), 443–452. https://doi.org/10.1109/TEMC.2009.2021616

Fan, Y., Lu, G., Jiang, R., Zhang, H., Li, X., Liu, M., et al. (2018). Characteristics of electromagnetic signals during the initial stage of negative rocket-triggered lightning. *Journal of Geophysical Research: Atmospheres*, *123*, 11,625–11,636. https://doi.org/10.1029/2018JD028744

Fuchs, F., Landers, E. U., Schmid, R., & Wiesinger, J. (1998). Lightning current and magnetic field parameters caused by lightning strikes to tall structures relating to interference of electronic systems. *IEEE Transactions on Electromagnetic Compatibility*, *40*(4), 444–451. https://doi.org/10.1109/15.736205

Gao, Y., Lu, W., Ma, Y., Chen, L., Zhang, Y., Yan, X., & Zhang, Y. (2014). Three-dimensional propagation characteristics of the upward connecting leaders in six negative tall-object flashes in Guangzhou. *Atmospheric Research*, *149*, 193–203. https://doi.org/10.1016/j.atmosres.2014.06.008

He, L., Azadifar, M., Rachidi, F., Rubinstein, M., Rakov, V. A., Cooray, V., et al. (2018). An analysis of current and electric field pulses associated with upward negative lightning flashes initiated from the Säntis tower. *Journal of Geophysical Research: Atmospheres*, *123*, 4045–4059. https://doi.org/10.1029/2018JD028295

Jiang, R., Qie, X., Wang, C., & Yang, J. (2013). Propagating features of upward positive leaders in the initial stage of rocket-triggered lightning. *Atmospheric Research*, *129-130*, 90–96. https://doi.org/10.1016/j.atmosres.2012.09.005

Kordi, B., Moini, R., Janischewskyj, W., Hussein, A. M., Shostak, V. O., & Rakov, V. A. (2003). Application of the antenna theory model to a tall tower struck by lightning. *Journal of Geophysical Research*, *108*, 4542. https://doi.org/10.1029/2003JD003398

Krider, E. P., & Noggle, R. C. (1975). Broadband antenna systems for lightning magnetic fields. *Journal of Applied Meteorology*, *14*(2), 252–256. https://doi.org/10.1175/1520-0450(1975)014<0252:BASFLM>2.0.CO;2

Lalande, P., Bondiou-Clergerie, A., Laroche, P., Eybert-Berard, A., Berlandis, J. P., Bador, B., et al. (1998). Leader properties determined with triggered lightning techniques. *Journal of Geophysical Research*, *103*(D12), 14,109–14,115. https://doi.org/10.1029/97JD02492

Lu, G., Zhang, H., Jiang, R., Fan, Y., Qie, X., Liu, M., et al. (2016). Characterization of initial current pulses in negative rocket-triggered lightning with sensitive magnetic sensor. *Radio Science*, *51*, 1432–1444. https://doi.org/10.1002/2016RS005945

Lu, W., Chen, L., Ma, Y., Rakov, V., Gao, Y., Zhang, Y., et al. (2013). Lightning attachment process involving connection of the downward negative leader to the lateral surface of the upward connecting leader. *Geophysical Research Letters*, *40*, 5531–5535. https://doi.org/10.1002/2013GL058060

Lu, W., Gao, Y., Chen, L., Qi, Q., Ma, Y., Zhang, Y., et al. (2015). Three-dimensional propagation characteristics of the leaders in the attachment process of a downward negative lightning flash. *Journal of Atmospheric and Solar-Terrestrial Physics*, *136*, 23–30. https://doi.org/10.1016/j.jastp.2015.07.011

Maslowski, G., & Rakov, V. A. (2006). A study of the lightning channel corona sheath. *Journal of Geophysical Research*, *111*, D14110. https://doi.org/10.1029/2005JD006858

Maslowski, G., & Rakov, V. A. (2013). Review of recent developments in lightning channel corona sheath research. *Atmospheric Research*, *129-130*, 117–122. https://doi.org/10.1016/j.atmosres.2012.05.028

Maslowski, G., Rakov, V. A., & Miki, M. (2011). Some inferences from radial electric fields measured inside the lightning-channel corona sheath. *IEEE Transactions on Electromagnetic Compatibility*, *53*(2), 390–394. https://doi.org/10.1109/TEMC.2011.2109063

Miki, M., Shindo, T., Rakov, V. A., Uman, M. A., Diendorfer, G., Mair, M., et al. (2006). Characterization of current pulses superimposed on the continuous current in upward lightning initiated from tall objects and in rocket-triggered lightning, paper presented at 28th International Conference on Lightning Protection (ICLP), ICLP, Kanazawa, Japan.

Rachidi, F., Janischewskyj, W., Hussein, A. M., Nucci, C. A., Guerrieri, S., Kordi, B., & Chang, J.-S. (2001). Current and electromagnetic field associated with lightning-return strokes to tall towers. *IEEE Transactions on Electromagnetic Compatibility*, *43*(3), 356–367. https://doi.org/10.1109/15.942607

Rakov, V. A., & Uman, M. A. (2003). *Lightning: Physics and effects*. Cambridge: Cambridge University Press.

Romero, C., Rachidi, F., Paolone, M., & Rubinstein, M. (2013). Statistical distributions of lightning currents associated with upward negative flashes based on the data collected at the Säntis (EMC) tower in 2010 and 2011. *IEEE Transactions on Power Delivery*, *28*(3), 1804–1812. https://doi.org/10.1109/TPWRD.2013.2254727

Takagi, N., Wang, D., Watanabe, T., Arima, I., Takeuchi, T., Simizu, M., et al. (1998). Expansion of the luminous region of the lightning return stroke channel. *Journal of Geophysical Research*, *103*(D12), 14,131–14,134. https://doi.org/10.1029/97JD02152

Thottappillil, R., & Rakov, V. A. (2001). On different approaches to calculating lightning electric fields. *Journal of Geophysical Research*, *106*(D13), 14,191–14,205. https://doi.org/10.1029/2001JD900150

Uman, M., Brantley, R., Lin, Y., Tiller, J., Krider, E. P., & McLain, D. K. (1975). Correlated electric and magnetic fields from lightning return strokes. *Journal of Geophysical Research*, *80*(3), 373–376. https://doi.org/10.1029/JC080i003p00373

Uman, M. A. (2001). *The lightning discharge*. Mineola, New York: Dover.

Wang, D., Rakov, V., Uman, M., Fernandez, M., Rambo, K., Schnetzer, G., & Fisher, R. (1999). Characterization of the initial stage of negative rocket-triggered lightning. *Journal of Geophysical Research*, *104*(D4), 4213–4222. https://doi.org/10.1029/1998JD200087

Wang, Z., Qie, X., Jiang, R., Wang, C., Lu, G., Sun, Z., et al. (2016). High-speed video observation of stepwise propagation of a natural upward positive leader. *Journal of Geophysical Research: Atmospheres*, *121*, 14,307–14,315. https://doi.org/10.1002/2016JD025605

Warner, T. A. (2010). Upward leader development from tall towers in response to downward stepped leaders, paper presented at 2010 30th International Conference on Lightning Protection (ICLP), IEEE.

Xu, Y., & Chen, M. (2013). A 3-D self-organized leader propagation model and its engineering approximation for lightning protection analysis. *IEEE Transactions on Power Delivery*, *28*(4), 2342–2355. https://doi.org/10.1109/TPWRD.2013.2263846

Zhou, H., Diendorfer, G., Thottappillil, R., Pichler, H., & Mair, M. (2012). Measured current and close electric field changes associated with the initiation of upward lightning from a tall tower. *Journal of Geophysical Research*, *117*, D08102. https://doi.org/10.1029/2011JD017269